International Journal of Mechanical, Industrial and Aerospace Sciences
ISSN: 2517-9950
Vol:5, No:1, 2011

Spray Combustion Dynamics under Thermoacoustic Oscillations

Wajid A. Chishty, Stephen D. Lepera and Uri Vandsburger

Abstract**—**Thermoacoustic instabilities in combustors have remained a topic of investigation for over a few decades due to the challenges it posses to the operation of low emission gas turbines. For combustors burning liquid fuel, understanding the cause-and-effect relationship between spray combustion dynamics and thermoacoustic oscillations is imperative for the successful development of any control methodology for its mitigation. The paper presents some very unique operating characteristics of a kerosene-fueled diffusion type combustor undergoing limit-cycle oscillations. Combustor stability limits were mapped using three different-sized injectors. The results show that combustor instability depends on the characteristics of the fuel spray. A simple analytic analysis is also reported in support of a plausible explanation for the unique combustor behavior. The study indicates that high amplitude acoustic pressure in the combustor may cause secondary breakdown of fuel droplets resulting in premixed pre-vaporized type burning of the diffusion type combustor.

Keywords**—**Secondary droplet breakup, Spray dynamics, Taylor Analogy Breakup Model, Thermoacoustic instabilities.

TABLE I
NOMENCLATURE

Symbol	Quantity	Units
A_a	cross-sectional area	[m^2]
D_o	initial droplet diameter	[m]
$F_{acoustic}$	acoustic pressure force	[N]
F_{drag}	drag force on droplet	[N]
m_o	droplet mass	[kg]
P'	acoustic pressure	[N/m^2]
Re_D	Reynolds Number	[-]
U_r	relative droplet velocity	[m/s]
μ_L	dynamic viscosity of liquid	[kg/m-sec]
ρ_a	density of gas	[kg/m^3]
σ_L	surface tension of liquid	[N/m]

I. Introduction

THE demand for high efficiency gas turbine engines for use in both power generation and propulsion has resulted in high compression ratios and high turbine inlet temperatures. In turn, the modern combustors are required to be designed to accommodate the rising operating pressures and temperatures. Higher combustor pressures and temperatures result in the formation of higher levels of nitrogen oxides (NOx).

Motivated by the environmental concern, low NOx combustor designs have been investigated by gas turbine manufacturers [1]. From the point of view of liquid-fueled gas turbines, one of these technologies is the Lean Direct Injection (LDI) combustor. In such combustors, fuel is directly introduced in the burner/combustor section, where it is simultaneously vaporized, mixed and burned with the combustion air. Because of reduced dimensions, simplicity and no unwanted flash back issues, even at elevated pressures and temperatures, LDI concept offers a greater potential for aircraft applications compared to other dry low NOx concepts.

However, LDI combustors may be highly susceptible to thermoacoustic oscillations under certain operating conditions. The oscillations may occur not only at lean operating conditions [2], but are possible over the entire operating range. This is so because combustors are high energy systems with weak acoustically-damped geometries and even a very small fraction of the heat release is sufficient to cause oscillations in the pressure fields. The acoustic pressure oscillations in turn affect the spray combustion dynamics via acoustic velocity oscillations causing oscillations in fuel spray vaporization [3], which is considered the rate controlling mechanism in such combustors.

This paper presents the experimental characterization of a kerosene-fueled test combustor operating in direct injection configuration. Some very unique operating characteristics under limit-cycle thermoacoustic oscillations are reported. The onset and sustenance of the thermoacoustic instabilities and the sensitivity of the combustor and the limit-cycle amplitude and frequency to changes in injector size are discussed. A simple analytical analysis is also presented to provide a plausible explanation for the reported combustor behavior.

II. Experimental Investigation

A. Experimental Setup

The experiments were conducted at Virginia Polytechnic Institute and State University. Experiments were performed under atmospheric pressure conditions on a cylindrical 75 kW LDI, swirl-stabilized combustor rig, fueled with kerosene [4]. An air inlet temperature of 293 K was maintained during all experiments. The combustor rig comprises three main sections: the combustor, the burner-plenum and the flow-conditioning section that houses the fuel and air supply lines. The sudden expansion (dump) combustion section was 1270 mm long with an internal diameter of 127 mm, while the flow-conditioning section was 864 mm long with an internal diameter of 76 mm. Optical access was provided on the combustors through three rectangular fused-silica windows. Combustion air was introduced in the combustor through a

45° axial swirler, which gives the air a geometric swirl number of 0.81. Fuel was introduced into the combustor via a full-cone pressure-swirl simplex injector. Pressure measurements were obtained using dynamic pressure transducers, which were mounted throughout the length of both the combustor and the flow-conditioning sections. The heat release rate measurements were made using a photo multiplier tube with suitable optics and signal conditioning to capture the OH* chemiluminescence. Temperature measurements were collected in the combustor and in the air and fuel feed lines. Data acquisition was provided using an 8-channel simultaneous sample and hold data-acquisition card and an anti-aliasing filter.

B. Stability mapping

Combustor performance was mapped over its complete operating range, which was dictated by the limitations imposed by the fuel injector and the fuel pump capacities, air supply capability and the thermal loading of the combustor. A solid-cone burner atomizer from Delavan, WDB-1.00 with a Flow Number (FN) of 3.42 [5] was used as the baseline injector.

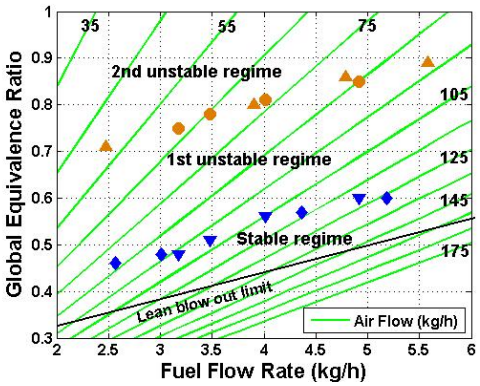

Fig. 1 Stability map of combustor's operating range using FN 3.42 injector.

Symbols ▼ and ● represent the transition to 1st and 2nd unstable regimes respectively when only air flow rate was varied. Symbols ♦ and ▲ indicate the same transitions when only fuel flow rate was varied

Fig. 1 depicts a typical stability map, over the range of tested conditions, in terms of fuel mass flow rate and Global Equivalence Ratio (GER). The lines running across the plot represent the corresponding mass flow rate of combustion air. At low GER the combustor was found to operate in a stable mode, characterized by a well-mixed and compact flame. As the GER was increased, the combustor became thermoacoustically unstable, entering what is labeled in Fig. 1 as the 1st unstable regime. This operationally unstable regime was characterized by a poorly-mixed, luminous flame surrounding diffusion burning of individual droplets or droplet clouds. An abrupt transition to the 2nd unstable regime was encountered when the GER was further increased towards stoichiometric. In this operating regime the flame appeared highly stretched and resembled a pre-vaporized premixed flame. The images of the flame appearance under the stable and the two unstable regimes are shown in Fig. 2.

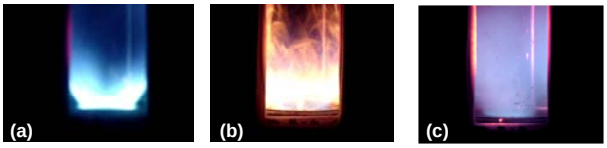

Fig. 2 Flame appearance in (a) Stable, (b) 1st unstable and (c) 2nd unstable operating regimes

As may be noted from Fig. 1, this GER dependent behavior of the combustor, transitioning between stable to 1st unstable to 2nd unstable modes, was found independent of the manner in which GER was varied. That is, either via changes in air flow rate with constant fuel flow rate; or changes in fuel flow rate keeping air flow rate constant; or changes in both air and fuel flow rates.

The evolution of thermoacoustic instability in the combustor with increasing GER is depicted in Fig. 3, where the power spectral densities of heat release rate and acoustic pressures in the combustor section are plotted. As may be noted, at a GER value of 0.4, although there is no preferred oscillations in the heat release rate (Fig. 3-a), nevertheless the mean thermal energy in the combustor is high enough to excite the combustor at its quarter-wave resonance frequency of 123 Hz (Fig. 3-b, some energy contents are also observed at the 1st harmonic frequency). At this operating condition, the acoustic losses in the combustor prevent the combustor from going unstable. These acoustic losses occur due to acoustic radiation at the open end, due to heat diffusion at the combustor walls and due to the presence of spray fuel in the combustor [6]. As the GER value is raised to 0.45, the amplitude of acoustic oscillations in the combustor also increases and the first sign of acoustic coupling with heat release rate is observed (spike indicated in Fig. 3-a) at a preferred frequency equal to the combustor resonance frequency. Any further increase in GER causes the acoustically driven heat release rate oscillations to fall in phase with the combustor pressure oscillations. Thus, making the combustor thermoacoustically unstable and exhibiting even larger pressure oscillations. With reference to the combustor stability map (Fig. 1) this GER limit signifies the boundary of the 1st unstable regime. Measurements taken well inside the 1st and 2nd unstable regimes of operation (at GER of 0.5 and 0.7 respectively) show the sharp peaks in pressure and acoustically driven heat release rate spectra. The presence of significantly prominent even harmonics indicate the presence of strong non-linear effects [7].

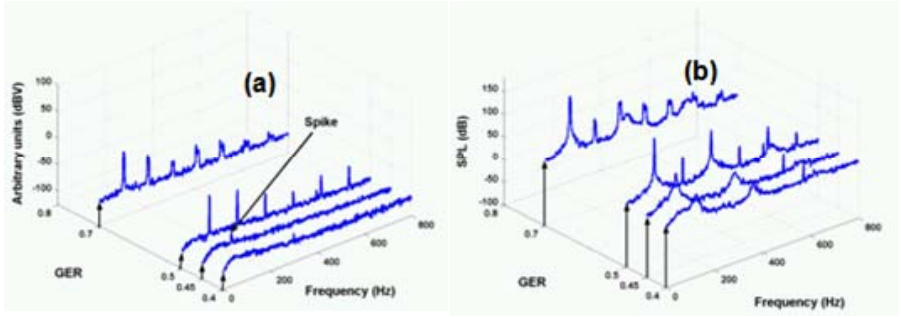

Fig. 3 Evolution of: (a) acoustically driven heat release rate; and (b) acoustic pressure in the combustor section

C. Characterization of Stability Regimes

The distinctive appearance of the flame in the three stability regimes (Fig. 2) was further characterized via pressure, temperature, acoustic velocity and heat release rate measurements. The FN 3.42 atomizer was used in all the reported experiments. The power spectral densities of acoustic pressure in the three regimes are shown in Fig. 4. Distinct behavior may be noted in the measured acoustic pressure profiles. The sound pressure level (SPL) at the fundamental frequency increases from 80dB in the stable operation to 161dB in the 1st unstable regime with resonance frequency shifting from 123 Hz to the limit cycle value of 118 Hz. The limit cycling is evident from the appearance of non-linear even-harmonic peaks in the pressure profiles. Higher acoustic modes also get excited as evident from the more prominent higher harmonic peaks. In the 2nd unstable regime the limit cycle frequency further shifts to a lower value of 100 Hz with a slight increase (to 167dB) in the sound amplitude. The reason for decrease in frequency in 2nd unstable regime is explained later in the paper. The even-harmonic peaks are much more prominent indicating strong presence of non-linear processes.

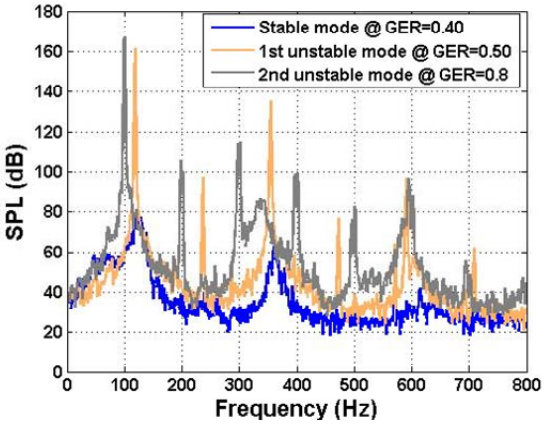

Fig. 4 Power spectral densities of combustor acoustic pressure in the three stability regimes

The changes in acoustic velocities in the combustor with the increase in GER from a lean limit towards stoichiometric are shown in Fig. 5. These velocities were calculated using acoustic pressure signals acquired from two closely placed wall-mounted pressure transducers in the flame zone. Also shown in Fig. 5 are the spray droplet velocities (relative to the advective co-flowing gas velocities). As may be noted, at higher GER, the acoustic velocities in the combustor reach very high amplitudes as compared to the droplet relative velocities.

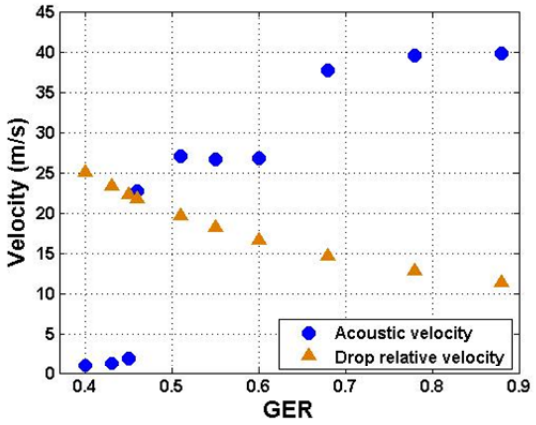

Fig. 5 Comparison between acoustic velocities and droplet relative velocities at different GER values

The temperature and the mean heat release rate profiles are shown in Fig. 6 and 7 respectively. The temperature profiles were measured in the flame zone and in the burner section, just upstream of the swirler-injector assembly. A sudden increase of about 200K in upstream temperature is observed when the combustor transitions to the 2nd unstable regime, indicating upstream movement of the flame front. Since this movement of the flame front influences (increases) the effective acoustic length of the combustor, this observation provides the explanation for the decrease in limit cycle frequency in the 2nd unstable regime. Also shown in Fig. 6 is a distinct drop in the flame zone temperature (measured at the combustor centerline) in the 2nd unstable regime. Corresponding drop in the mean heat release rate were also observed as shown in Fig. 7. The observation on the decrease of mean heat release rate qualitatively verifies the presence of distributed and strained reaction zone in the 2nd unstable regime. It may be mentioned here that the heat release rate

measurements are based on global OH* chemiluminescence signal averaged over a flame area equivalent to the viewing area of the combustor window.

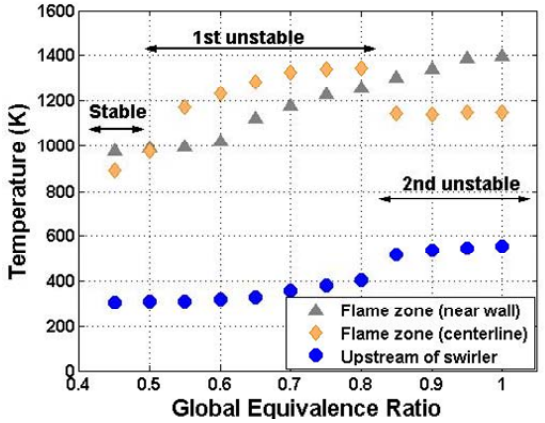

Fig. 6 Temperature profiles in the combustor and burner

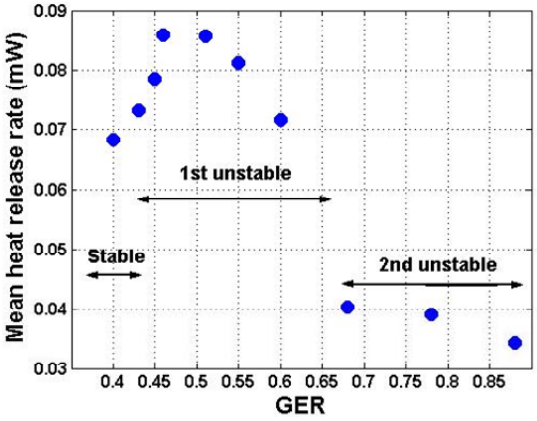

Fig. 7 Mean heat release rate at different GER values

D.Influence of Spray Chracteristics

In order to investigate the effect of atomization i.e., changes in Sauter Mean Diameter (SMD) on the combustor's stability behavior, mapping was also conducted using injectors of two other Flow Number (FN), as listed in Table 1. Spray characterization for the three injectors was conducted using Phase Doppler Anemometry (PDA) under non-reacting flow conditions. The results are summarized in Fig. 8. As may be noted, use of higher FN injector results in higher SMD at a fixed fuel injection pressure.

TABLE I
SPECIFICATIONS OF THE INJECTORS USED IN THE EXPERIMENTS

Atomizer	Mass flow rate @ 0.862 MPa [kg/h]	Orifice size [mm]	FN*
WDB-0.75	2.380	0.234	2.56
WDB-1.00	3.174	0.280	3.42
WDB-1.50	4.761	0.330	5.13

* Flow Number (FN) calculated using Ref. 5.

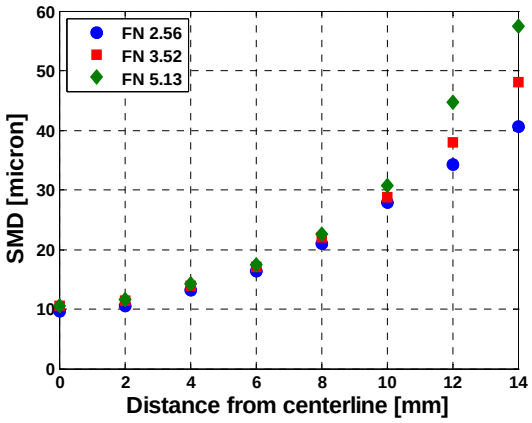

Fig. 8 Droplet size distribution of three injectors: FN 2.56; FN 3.42; and FN 5.13 at injection pressure of 0.862 MPa

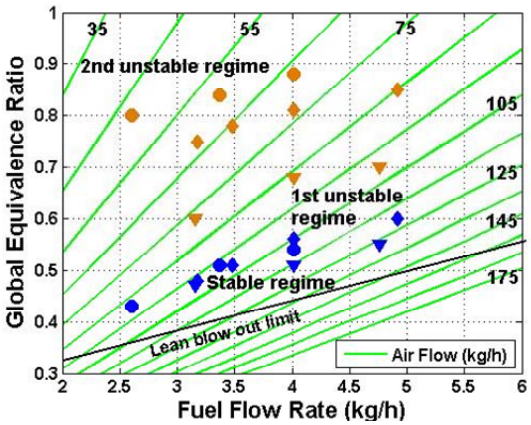

Fig. 9 Stability map showing combustor's transition to the two unstable regimes using different FN injectors. ● for FN 2.56, ♦ for FN 3.42 and ▼ for FN 5.13

Combustor stability mapping was conducted using all the three FN injectors. Results are compared in Fig. 9, which indicates the transitions from stable to unstable regimes for the three injectors. As may be noted, the 1st unstable boundary was found to be independent of the injector type, while distinct differences were observed at the 2nd unstable boundary. The transition to the 2nd unstable regime was found delayed (i.e., occuring at higher GER) when injectors with finer SMD (lower FN) were used, while for larger SMD injectors (higher FN) a shrinkage in the 1st unstable region was observed.

III. Analytical Investgation of Spray-Acoustics Interaction

The experimental observation of the combustor transitioning to the 2nd unstable regime and the dependence of this transitioning on the injector characteristics were further investigated.

As seen in Fig. 5, the acoustic levels under unstable combustor conditions reach very high amplitudes. Review of experimental work by Anilkumar et al. [8], indicates that such high acoustic levels may cause a breakup of droplets. Based on this premise, it was hypothized that the combustor's transition from the 1st to the 2nd unstable regime was due to acoustically induced secondary breakup of the spray droplets. An analytical study was therefore conducted to test this hypothesis and investigate the spray–acoustics interaction. .

Studies show that secondary breakup is almost always preceded by deformation and oscillation of the droplet [9]. As the aerodynamic forces (resulting from droplet relative velocities) intensify relative to surface tension and viscous forces, the droplet is no longer able to maintain its spherical shape. This results in oscillatory deformation, which is followed by breakup.

A widely used model that has been successfully used in comprehensive spray combustion codes is the Taylor Analogy Breakup (TAB) model proposed by O'Rourke and Amsden [10]. The TAB model has been formulated based on the assumption that the droplet oscillatory deformation is analogous to a damped forced harmonic oscillator like a spring-mass- damper system. In the model, the spring restoring force and the damping force are replaced by the surface tension and viscous forces in the droplet respectively, while the external force on the mass is substituted by the gas aerodynamic force. Spherical symmetry of the droplet is also assumed. The model has been found to predict sizes and velocities of the resulting drops that are consistent with the experimental measurements. The TAB model was used in the present study with a modification to include instantaneous variations in droplet drag due to changes in drop shape, as suggested in Ref. 11.

Thus for a droplet, the 1-D differential equation is of the form,

$$m_D\ddot{y}+\mu_L D_o\dot{y}+\sigma_L y=F_{ext} \tag{1}$$

In the equation, y represents the oscillatory deformation at the north and south poles of the droplet, as shown in Fig. 10. The external force F_{ext} is made up of an aerodynamic drag force on the droplet due to its velocity relative to the gas phase velocity and a pressure force, which in the present study was considered due to acoustic pressure. Thus,

$$F_{ext}=F_{acoustic}-F_{drag}=P'A_C-\frac{1}{2}\rho_g|U_r|^2C_dA_C \tag{2}$$

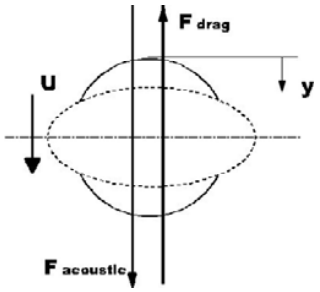

Fig. 10 Spherical droplet treated as a harmonic oscillator

Substituting for F_{ext} in Equ. 1; expressing droplet mass in terms of its diameter; and normalizing the deformation, y by the droplet initial diameter a non-dimensional form of Equ 1 is obtained,

$$\ddot{z}+\left(\frac{6\mu_L}{\pi D_o^2\rho_L}\right)\dot{z}+\left(\frac{6\sigma_L}{\pi D_o^3\rho_L}\right)z=\left(P'-\frac{1}{2}\rho_g|U_r|^2C_d\right)\left(\frac{3}{2D_o^2\rho_L}\right) \tag{3}$$

Here, z is the non-dimensional deformation and C_d is the drag coefficient for a deforming sphere. To account for the changes in droplet shape due to deformation [11], the drag coefficient is given by,

$$C_d=\frac{64}{\mathrm{Re}_D}(1+2.632z) \tag{4}$$

A close form solution of Equ. 3 may be obtained by specifying initial values of z and $\dot{z}$. The droplet breakup criterion was set to be $z_{ss} \geq 0.5$, where, z_{ss} is the steady state value of z.

For the presented results, droplet velocity of 5 m/s was assumed. The temperature values at which the liquid fuel properties were determined as well the acoustic pressure and the advective flow values were kept the same as in the reacting flow experiments for a GER of 0.6 (refer Fig. 5 and Fig. 7). Using the solution of Equ. 3, time traces of non-dimensional deformation of four different droplet sizes are shown in Fig. 11. Under the influence of a one-dimensional acoustic field, the droplet behaves like a harmonic oscillator and demonstrates an oscillatory deformation. It may be noted that larger droplets demonstrate higher oscillations in their deformation with lesser degree of damping as compared to the smaller droplets. If the influence of acoustic pressure force is dominant relative to the external drag force and the internal restoring surface tension force, the steady state deformation may exceed the breakup criterion limit of 0.5 and droplet breakup occurs. Thus larger droplets were found to be more susceptible to deformation due to the presence of high acoustic pressure levels.

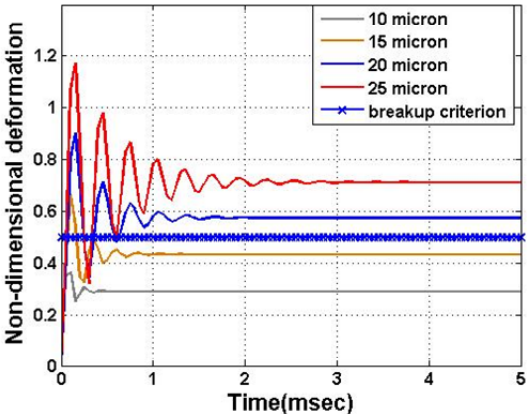

Fig. 11 Oscillatory deformation of different sized droplets under the same external acoustic and other operating condition

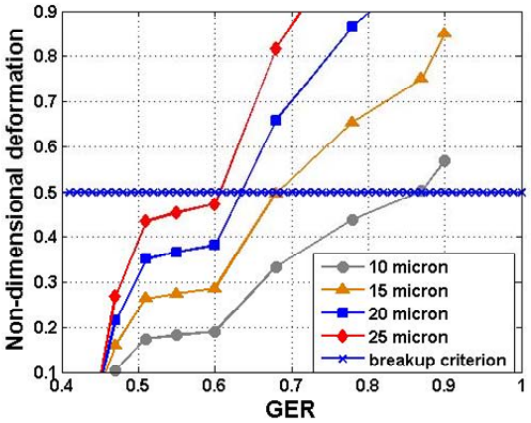

Fig. 12 Occurrence of acoustically induced secondary droplet breakup at the combustor operating conditions

For the same four droplet sizes, a number of such simulations were performed over the range of experimental operating conditions. The results of the analysis are summarized in Fig. 12 where the non-dimensional deformations are plotted versus the GER to how the influence of combustor acoustics on the droplet breakup. The plot shows that the smaller the mean size of the droplets, the higher the critical value of GER at which the breakup occurs. These results qualitatively verify the experimental findings shown in Fig. 9, where, for a smaller FN injector (with finer SMD) the 2nd unstable regime (characterized by droplet secondary breakup) is reached at a higher value of GER.

IV. Summary

Experimental investigations were conducted to characterize a liquid-fueled direct injection combustor under thermoacoustic oscillations. Depending on the GER and the relative level of acoustic dominance, it was observed that the combustor demonstrates three operational regimes: Stable operation at lower GER and two very distinct unstable regimes at higher GER. Under transition to unstable conditions, the limit cycle frequencies were found to shift to lower values compared to the resonance frequency of the combustor. Temperature measurements indicated that the flame front moved upstream in the 2nd unstable operational mode of the combustor. A sudden decrease in mean heat release rate also occurred during this transition, which qualitatively indicates the presence of distributed and strained reaction zone in the 2nd unstable regime. Acoustic velocity measurements showed that the magnitude of acoustic velocities in the combustor was comparable to the relative convective flow velocities in the 1st unstable regime and were four times higher in the 2nd unstable regime.

The regions of acoustically unstable operation under the 1st and the 2nd unstable modes were found to depend on the atomizing capacity of the fuel injectors i.e., the mean droplet diameter. Smaller SMD delayed the transition to 2nd unstable regimes to occur at relatively higher GER, while larger SMD caused shrinkage in 1st unstable regime. About 80dB rise in SPL was observed under unstable combustor operation. The maximum pressure oscillations observed at any GER were 4.5% relative to the mean pressure in the combustor. It was found that the combustor acoustics was the driving mechanism of the thermoacoustic instability in the combustor.

Analytical investigation using TAB Model showed that high level of acoustic pressures may cause secondary droplet breakdown, especially when the relative advective velocities are low compared to the acoustic velocities. This provided a plausible explanation for combustor operation transitioning to the 2nd unstable regime.

Acknowledgment

The work was funded by NASA Glenn Research Centre, under Contract NRA-01-GRC-02. The authors appreciate the efforts of Mr. Mike Player of National Research Council Canada for providing the injector characterization data.

References

[1] J. C. Solt, J. Tuzson, Proceedings of 1993 ASME IGTI Conference Paper 93-GT-270, 1993.
[2] T. Lieuwen, B. T. Zinn, AIAA 36th Aerospace Sciences Meeting & Exhibit Paper 98-0641, 1998.
[3] A. Y. Tong, W. A. Sirignano, Journal of Propulsion and Power 5(3) (1989) 257-261.
[4] W. A. Chishty, *Effects of Thermoacoustic Oscillations on Spray Combustion Dynamics with Implications for Lean Direct Injection Systems*, PhD thesis, Virginia Polytechnic Institute and State University, Blacksburg, VA, USA, 2005.
[5] A. M. Mellor, Design of Modern Turbine Combustors, Academic Press Limited, 1990.
[6] C. Clanet, G. Searby, P. Clavin, Journal of Fluid Mechanics 385 (1999) 157-197.
[7] S. Dowson, J. Fitzpatrick, Journal of Sound and Vibration 230(3) (2000) 649-660.
[8] A. V. Anilkumar, C. P. Lee, T. G. Wang, NASA Conference Publication 3338, (1996) 559–564.
[9] R. Schmehl, G. Klose, G. Maier, S. Wittig, S., NATO RTO Gas Turbine Engine Combustion, Emissions and Alternate Fuels, 1999.
[10] P. J. O'Rourke, A. A. Amsden, SAE Technical Report 872089, 1987.
[11] J.-H. Park, Y. Yoon, Atomization and Sprays 12 (2002) 387– 401.